Renewable and environmentally friendly of “red shoots” leaves biomass-based carbon electrode materials for supercapacitor energy storage

Renewable and environmentally friendly of "red shoots" leaves biomass-based carbon electrode materials for supercapacitor energy storage

Erman Taer[1,*], Aprilia Susanti[1], Rika Taslim[2], Apriwandi[1]

[1] Department of Physics, University of Riau, 28293 Simpang Baru, Riau, Indonesia
[2] Departement of Industrial Engineering, State Islamic University of Sultan Syarif Kasim, 28293 Simpang Baru, Riau, Indonesia

[*]erman.taer@lecturer.unri.ac.id

Abstract. Porous activated carbon monolith derived from renewable and environmentally friendly biomass of "red shoots" leaves (*Syzygium oleana*) was prepared for electrode material of supercapacitors. The raw materials were converted into biochar by using $ZnCl_2$ impregnated and one-stage integrated pyrolysis. The samples were chemically activated using the 1 M $ZnCl_2$, which was then converted into monolith/pellet by using a hydraulic press. The carbon monolith were then one-stage integrated pyrolysis both carbonization and physical activation. This study is focused in different carbonization temperature including 500 °C, 600 °C and 700 °C. The reduction of density in the activated carbon monoliths have been reviewed as physical properties. In addition, the XRD and FTIR characterization also reviewed. Based on this, the activated carbon monolith from "red shoots" leaves biomass for supercapacitors deliver a high specific capacitance of 138.5 F g^{-1} in 1 M H_2SO_4 aqueous electrolyte at low scanning rate of 1 mVs^{-1}. This results demonstrate the successfully conversion "red shoots" leaves (*Syzygium oleana*) biomass into renewable and environmentally friendly electrode supercapacitor energy storage.

1. Introduction

Environmental pollution due to the increasing consumption of fossil energy sources is an urgent global problem today. Therefore, a sustainable energy source that is environmentally friendly is needed to reduce the impact of environmental destruction. Several alternative energy sources offered by researchers include solar energy, wind energy, tidal energy, and biomass energy [1,2]. However, switching the main energy source to alternative energy requires a relatively high cost. In addition, alternative energy sources are not always available all the time, thus requiring energy storage devices. In the last decade, researchers have suggested that electrochemical processes are the most ideal form of energy storage and conversion especially in this case are supercapacitors [3,4]. Supercapacitors can bridge the gap in several other energy storage devices such as conventional capacitors and batteries [5,6]. Furthermore, supercapacitors have a number of advantages, such as high power density, excellent energy density, and good cycle stability [7,8]. The EDLC-type supercapacitor is considered the most promising candidate. However, due to the electrostatic surface charging mechanism, this device is subjected to limited specific energy. Electrode material modification is the main step taken by researchers to increase the specific energy of the EDLC-type supercapacitor. Carbon materials such as graphene [9,10], carbon nanotubes [11,12], mesoporous carbon [13], and carbon nanofibers [14–16]

have been used as supercapacitor electrode materials, and show excellent performance in enhancing supercapacitor performance. However, their high production costs limit their practical application. Therefore, low-cost carbon electrode preparation for supercapacitors remains a challenge. Recently, porous carbon materials derived from biomass wastes with various combinations of pore structures have attracted a lot of attention due to their abundant, cheaper, and renewable resources [2,17,18]. In this study, we used red shoots as the raw material of activated carbon for the supercapacitor electrodes. Red shoots waste was converted into biochar using a relatively uncomplicated method through impregnation of $ZnCl_2$ and pyrolysis. The pyrolysis process includes carbonization and physical activation in N_2 and CO_2 gas environment. Furthermore, activated carbon is prepared in a monolith or pellet form without the addition of any adhesive material. All analysed samples showed good amorphous structure to improve the symmetrical supercapacitor performance. Moreover, the maximum capacitive properties found were 141 F g^{-1} in 1 M H_2SO_4 electrolyte.

2. Material and methods

2.1. Preparation of activated carbon monolith

The activated carbon monoliths were prepared by using three steps processes including initial treatment, chemical activation, and pyrolysis process. Initial treatment was done by collected, cleaned, and dried the red shoots as biomass waste. Red shoots leaves are collected from University of Riau area. Next, the samples were cleaned and continued to dried by sunlight and oven vacuum at a temperature of 110 ºC. Then, the samples were pre-carbonized at a temperature of 250 ºC. Subsequently, the precursors change into carbon powder by using mortal, pestle, and milling tools. To obtain the homogenous powder, the samples were sieving in 35 µm size. Zink chloride ($ZnCl_2$) in 1 M concentration was chosen as chemical activation reagent. Moreover, the powder samples were converted into pellet or monolith form without addition of adhesive materials by using hydraulic press. Subsequently, 20 monolith samples were pyrolysis by using one-stage integrated pyrolysis both carbonization and physical activation in N_2/CO_2 gas atmosphere [19]. The temperature, the heating rate, and the nitrogen gas flow are the significant parameters in this stage and in this study we selected three different carbonization temperatures of 500, 600, and 700 ºC. Based on this different temperature, all samples were labelled PM500, PM600, and PM700. The physical activation was performed in CO_2 gas environment at high temperature of 900 ºC in 2,5 h [20]. Next, the monolith samples were neutralized by using distillate water. In detail, the preparation sample is shown in Figure 1.

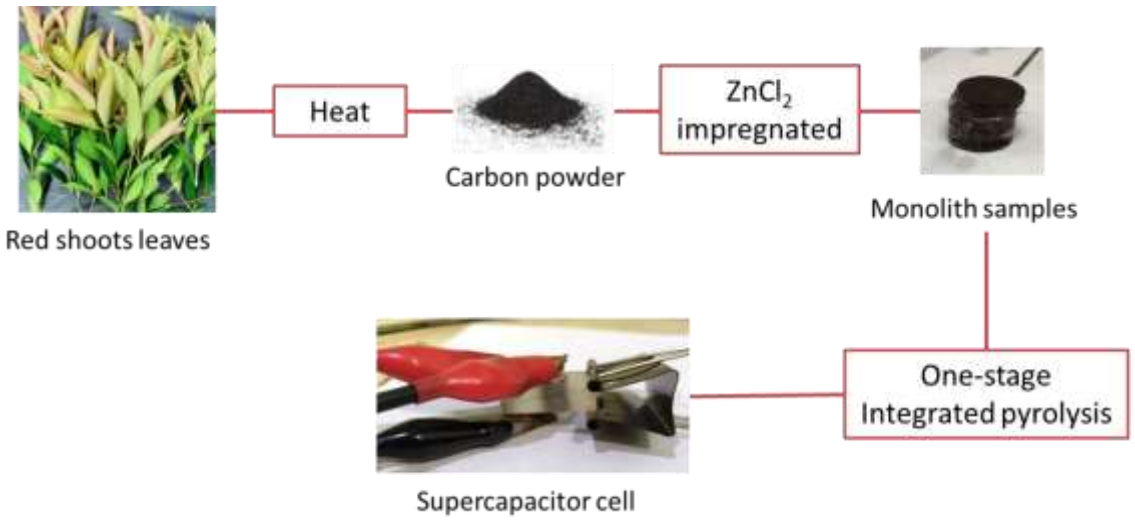

Fig. 1. The preparation of activated carbon monolith for electrode supercapacitor

2.2. Characterizations

The 20 monolith samples were evaluated based on the reduction of dimensions including mass, thickness, diameter and density. Fourier transform infrared spectrometry (FTIR, Shimadzu, IR Prestige-21) was performed to determine the presence of various functional groups of the activated carbon monolith. Furthermore, the microstructure behaviour was characterized by using X-ray diffraction (XRD, Shimadzu 7000) technique in the 2θ angle range of 10-60° with a source of Cu-Kα radiation (Kα=1 .5418 Å). In addition, interlayers spacing (d_{002} and d_{100}) were obtained by using Bragg's Law while the microcrystalline dimension (L_c and L_a) were calculated by Debye-Scherer Equation. Moreover, the capacitive performance of the symmetric supercapacitor was evaluated by using cyclic voltammetry (CV, UR Rad-Er 5841 instrument) technique in two electrode system with 1M H_2SO_4 as electrolyte. The supercapacitor cell was rearrangement with sandwich type consist of two electrode from activated carbon monolith derived from red shoots leaves, duck eggshell membrane as separator [21], and 1M H_2SO_4 as electrolyte. The specific capacitance was evaluated by using standard formula [22,23].

3. Result and Discussions

Chemical activation and pyrolysis processes are the main steps required to convert biomass waste into carbon fixed, including converting red shoots leave to monolithic activated carbon. All samples in the form of monoliths are a change in dimensions including mass, diameter, and thickness. It could be used to calculate the density before and after the one-stage pyrolysis process. The pyrolysis process which includes carbonization and physical activation begins at room temperature to a high temperature of 900 °C. In this process, the water content, volatile, complex compounds including cellulose, hemicellulose, and lignin decompose to a temperature of 600 °C [24,25].

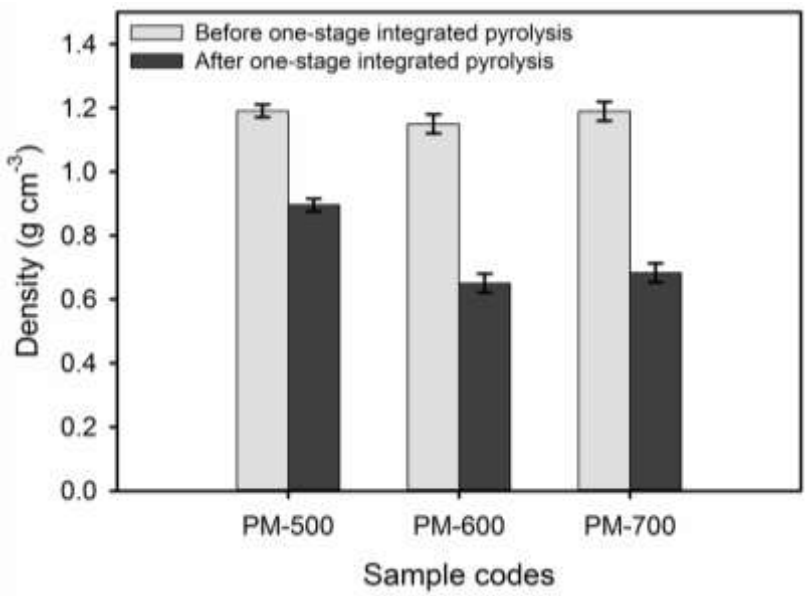

Fig 2. The reduction of density before and after pyrolysis

Furthermore, the temperature increases to 900 °C causing the formation and expansion of pores in the sample [26]. This phenomenon certainly reduces the mass, thickness, and diameter of the monolith sample and causes the density of the monolith to decrease. Figure 2 shows the density reductions for the PM500, PM600, and PM700. Before pyrolysis, the sample density values were 1.1909, 1.1502, and 1.1893 $cm^3\ g^{-1}$ for PM500, PM600, and PM700, respectively, with a mean standard deviation of 0.25. This density value decreased after the pyrolysis process as high as 0.8960, 0.6509, and 0.6834 $cm^3\ g^{-1}$ for PM500, PM600, and PM700, respectively. This is certainly due to the evaporation and

decomposition of chemical and volatile compounds in the sample. Furthermore, the difference in carbonization temperature in the sample affects the density value after the pyrolysis process. Increasing the carbonization temperature from 500 °C to 600 °C could decrease the density value from 24.76% to 43.40%, indicating that the decomposition of chemical compounds has succeeded in increasing the formation of new pores on activated carbon. Moreover, increasing the temperature until 700 °C did not showed a significant effect on the decrease in density. This analysis is correlated with the capacitive properties of the electrode which shows its best performance at a temperature of 600 °C.

The microstructure properties are mainly evaluated by using X-ray diffraction (XRD) technique. Figure 3 shows the XRD pattern of the monolith activated carbon based on the different carbonization temperatures of 500, 600, and 700 °C. The XRD curve clearly shows two wide peaks at an angle of 2θ=24-25º and 2θ=43-44º which refers to the reflection plane of (002) and (100), indicating a predominantly amorphous structure of carbon [27–29]. Furthermore, the broadening peaks in the (002) reflections corresponding to a highly amorphous structure while the (100) reflections confirm a small amount of hexagonal graphite structures. Moreover, the application of the carbonization temperature from 500 to 600 causes attenuation of the peak width as shown on the XRD curve. In addition, the peak width at 2θ = 24.036º and 2θ = 43.131º shifted to a larger direction up to 2θ = 25,238 º and 2θ = 44.050 º, as shown in Table 1. This phenomenon confirms that the increase in carbonization temperature from 500 °C to 600 °C suggests that the amorphous of activated carbon monolith increased with the increasing carbonization temperature. In addition, several sharp peaks were also seen, especially at angles 29º, 37º and 39º. This indicates that there are crystal elements and compounds in samples such as SiO_2 (JCPDS No. 89-1668), MgO (JCPDS No. 82-1690), and ZnO (JCPDS No. 79-2205). These compounds contribute as redox and faradaic to the supercapacitor electrodes.

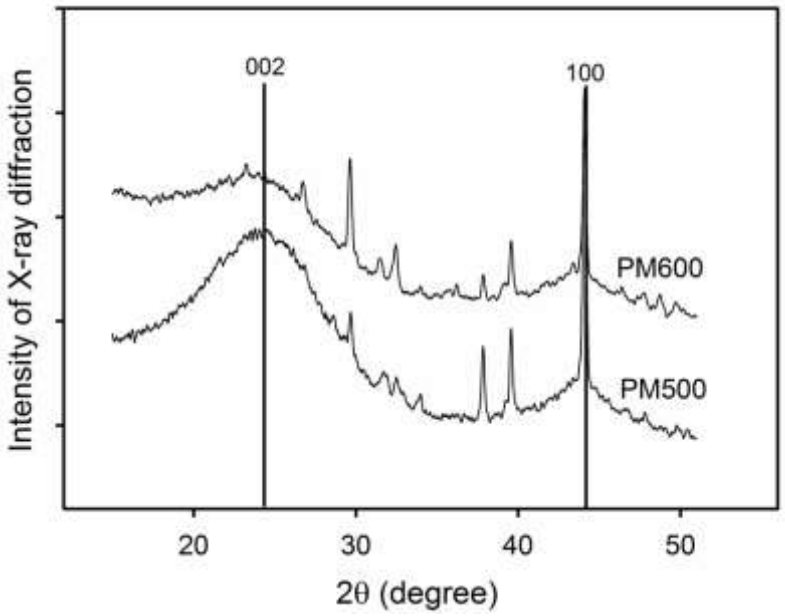

Fig 3. XRD pattern of the PM500 and PM600 samples

The interlayer spacing (d_{002} and d_{100}) and microcrystalline dimensions (L_c and L_a) were evaluated using the Braggs law and Debye-Scherer equation, as shown in Table 1. The d_{002} and d_{100} showed normal values for the amorphous carbon derived from biomass waste materials. A similar value was found in previous studies such as activated carbon made from durian shell [20], empty fruit bunch palm oil [30], and acacia leaves [31]. Furthermore, L_c value is considered to affect the surface area of activated carbon electrodes. Based on the empirical formula that has been previously reported [32,33],

the value of L_c is inversely proportional to the surface area, meaning that a small L_c has a high surface area and certainly increases the performance of the supercapacitor electrode. This means that the PM600 sample is predicted to have a higher surface area than the PM500. This is consistent with the density analysis previously presented above.

Table 1. The interlayer spacing (d_{002} and d_{100}) and microcrystalline dimensions (L_c and L_a) of the activated carbon monolith

Monolithic Carbon	$2\theta_{002}$ (˚)	$2\theta_{100}$ (˚)	d_{002} (Å)	d_{100} (Å)	L_c (Å)	L_a (Å)
PM500	24.036	43.131	3.699	2.095	14.912	48.079
PM600	25.238	44.050	3.525	2.054	10.918	45.382

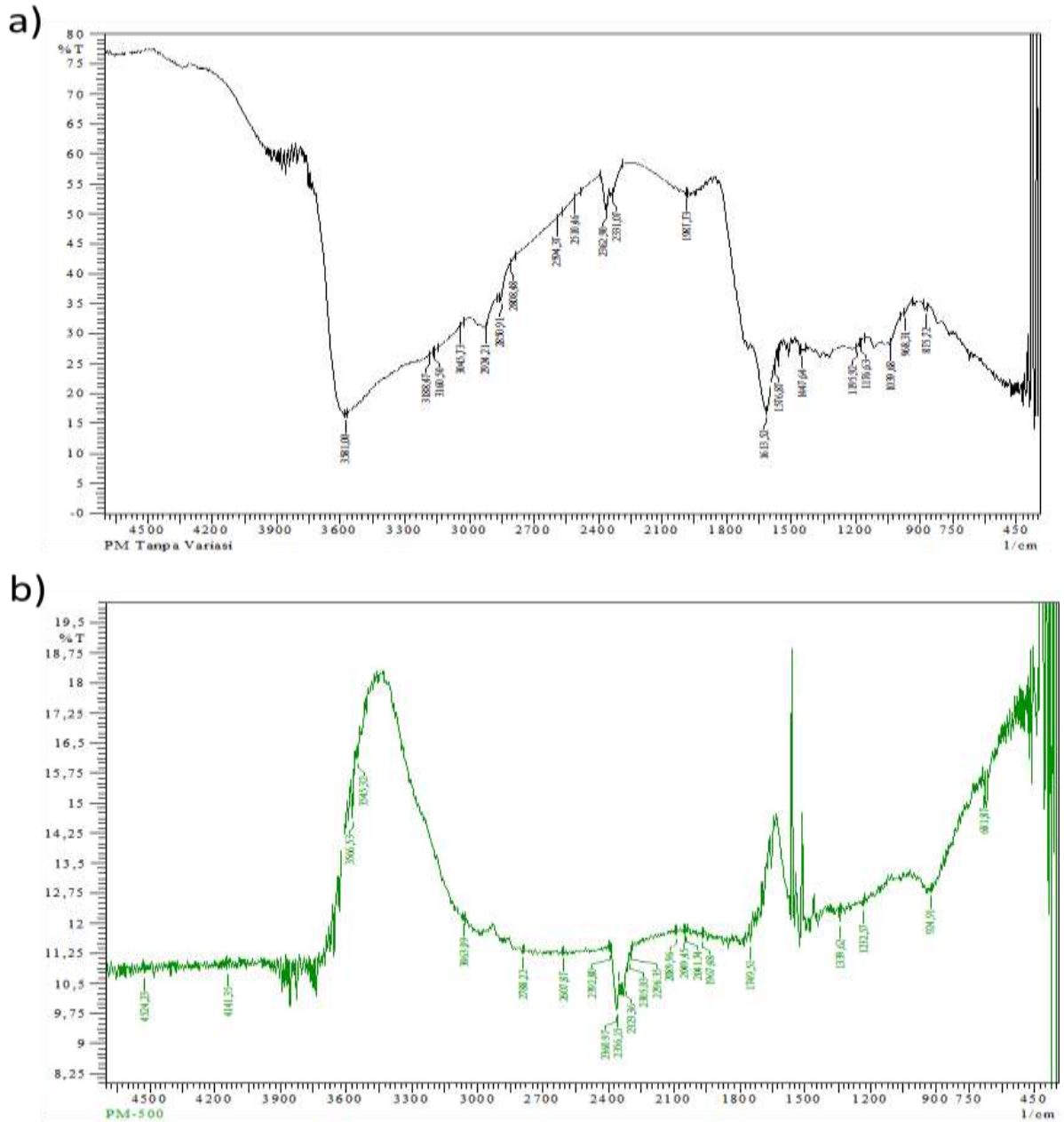

Fig. 4. FT-IR profile for (a) pure red shoots powder, and (b) PM500

Figure 4(a) shows the FT-IR spectrum profile of the red shoot leaves sample at a wavelength of 450-4500 cm^{-1}. The highest peak of the spectrum is at 3581 cm^{-1} which belongs to the hydroxyl ν (O-H) group. In addition, a wavenumber 2924.21 cm^{-1} indicates the alific functional group (C-H). Furthermore, the wavenumber 1613.52 cm^{-1} shows the presence of carbonyl stretching, and wavenumber 1176.63 cm^{-1} showed the presence of ether stretching.

Figure 4 (b) and Figure 5(a-b) performed the FTIR spectrum of PM500, PM600, and PM700, respectively. In the wavelength range of 3100-3600 cm^{-1} exhibit the hydroxyl functional group ν (OH), which in each sample in the peak of this functional group decreases due to the carbonization process. The numbers 2788.22 cm^{-1}, 2736.14 cm^{-1}, and 2908.78 cm^{-1} indicate the functional group (C-H). In the wavelength range of 1700-1870 cm^{-1} shows the carbonyl functional group (C=O). In the 1100-1200 cm^{-1} wavelength range, it shows the existence of the functional group ν (C-O). Furthermore, Figure 4 b-d also performed the high percentage of transmittance of each sample, where samples with PM 500 have a high percentage of transmittance in the carboxyl functional group (C=O), which indicates that PM 500 has more pure carbon than other samples. The hydroxyl functional group in the PM 600 sample has a higher percentage of transmittance than the other 2 samples, this is what makes the PM 600 sample have a lower density than the two samples.

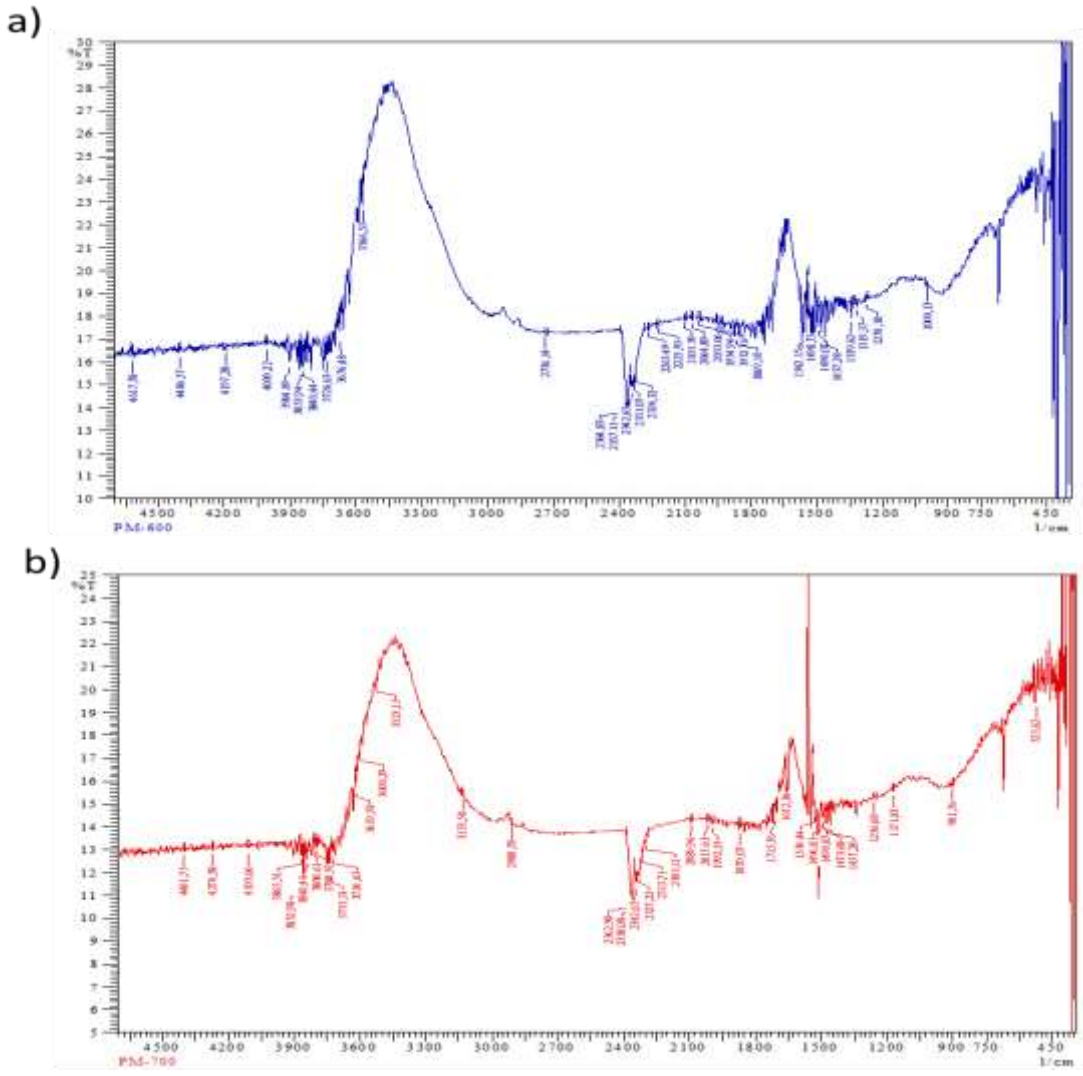

Fig. 5. FT-IR profile for (a) PM600, and (b) PM700

The electrochemical properties of the supercapacitor electrode of red shoots leave waste were evaluated by using the Cyclic Voltammetry (CV) method. The CV data could be used to determine the specific capacitance (C_{sp}) of a supercapacitor electrode. The results of the CV measurement are curves of charge current density and discharge current density against a potential window of 0-1.0 V with a scanning rate of 1 mV s^{-1}. The CV profile for activated carbon monolith based on different temperature of 500, 600, and 700 was shown in Figure 6. The CV curve performed a quasi-rectangular shape indicating normal EDLC behaviour for the electrode material [34,35]. Furthermore, the current density spikes could be reviewed at a voltage potential of 0.3-0.4 V, confirming that the sample has pseudo-capacitance properties contributed by the heteroatoms in the sample. Based on the standard equation, the specific capacitances are 122 F g^{-1}, 141 F g^{-1}, and 135 F g^{-1} for PM500, PM600, and PM700 samples, respectively. Increasing the carbonization temperature from 500 ºC to 600 ºC significantly improved the specific capacitance from 122 F g^{-1} to 141 F g^{-1}. This phenomenon was confirmed by the density and microcrystalline dimension properties discussed earlier which stated that the PM600 sample had better porosity and amorphous features than other samples. A further increase in carbonization temperature from 600 ºC to 700 ºC indicates a reduced capacitive from 141 F g^{-1} to 135 F g^{-1}, suggesting that well-formed pores at 600 ºC experience expansion at a higher temperature and cause a reduction in surface area. This certainly affects the performance of the sample working electrode.

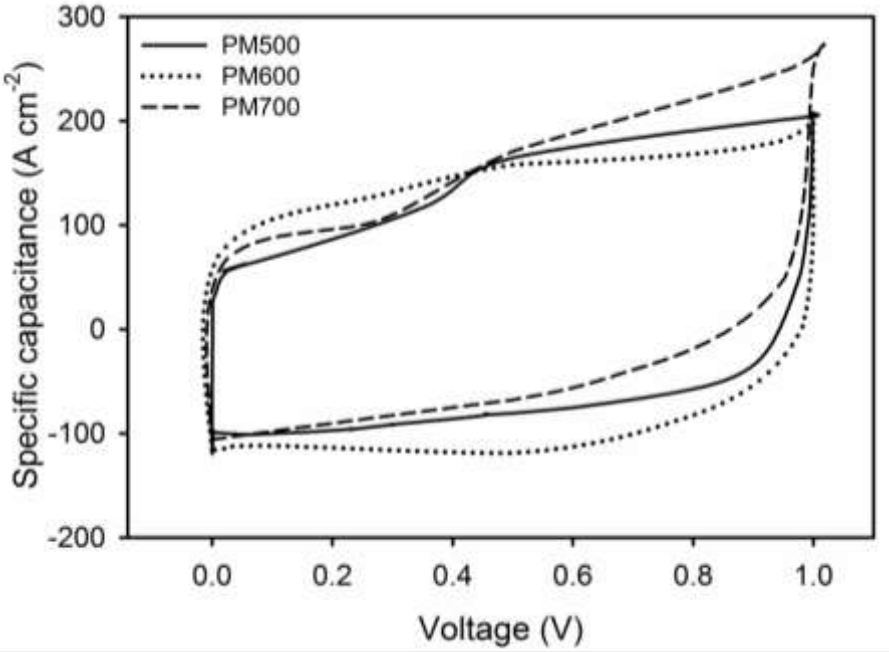

Fig .6. The CV profile of PM500, PM600 and PM700

In addition, the capacitive performance was also tested at different scanning rates including 1, 2, 5 and 10 mV s^{-1} for PM500, PM600, and PM700, respectively. The specific capacitance resulting from this evaluation is shown in Figure 7. The specific capacitance tends to be reduced as the scanning rate increases from 1 to 10 mV s^{-1} due to could reduce the ion diffusion time on the electrode surface. Furthermore, all samples still maintained their specific capacitance of 55%, indicating that the samples had relatively good conductivity.

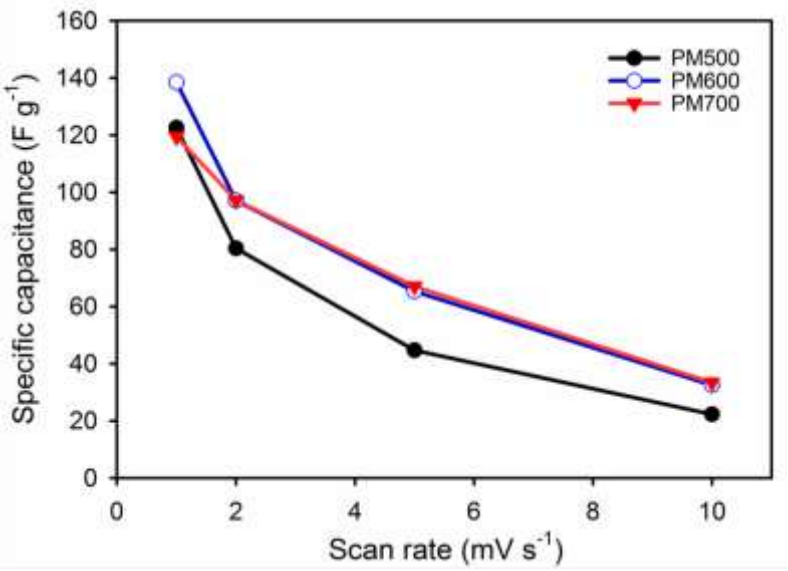

Fig. 7. The graph of specific capacitance vs. scanning rate for all samples

4. Conclusion

The "red shoots" leave (*Syzygium oleana*) activated carbon for electrode material were synthesized by $ZnCl_2$ impregnated followed by one-stage integrated pyrolysis both carbonization and physical activation. The different carbonization temperatures of 500, 600, and 700 ºC are the main focus of this study. When used as electrode materials for supercapacitor, the activated carbon monolith performed high capacitive behaviour for the supercapacitor energy storage was associated with the contribution of reduction of density and amorphous nature. Furthermore, symmetrical supercapacitor fabricated by 600 ºC carbonization temperatures has the highest specific capacitance of 141 F g^{-1} as well as a stable value with 55% in 10 mv s^{-1} at 1 M H_2SO_4 electrolyte. This results in providing new material sources with a simple method of activated carbon for the electrode material as a high-performance energy storage system.

5. References

[1] Fitra M, Daut I, Gomesh N, Irwanto M and Irwan Y M 2013 Dye solar cell using Syzigium Oleina organic dye *Energy Procedia* **36** 341–8
[2] Mensah-Darkwa K, Zequine C, Kahol P K and Gupta R K 2019 Supercapacitor energy storage device using biowastes: A sustainable approach to green energy *Sustain.* **11**
[3] Zhai Y, Dou Y, Zhao D, Fulvio P F, Mayes R T and Dai S 2011 Carbon Materials for Chemical Capacitive Energy Storage *Adv. Mater.* **23** 4828–50
[4] Liu T, Liu J, Zhang L, Cheng B and Yu J 2020 Construction of nickel cobalt sulfide nanosheet arrays on carbon cloth for performance-enhanced supercapacitor *J. Mater. Sci. Technol.* **47** 113–21
[5] Poonam, Sharma K, Arora A and Tripathi S K 2019 Review of supercapacitors: Materials and devices *J. Energy Storage* **21** 801–25
[6] González-García P 2018 Activated carbon from lignocellulosics precursors: A review of the synthesis methods, characterization techniques and applications *Renew. Sustain. Energy Rev.* **82** 1393–414
[7] Burke A 2000 Ultracapacitors: why, how, and where is the technology *J. Power Sources* **91** 37–50
[8] Pandolfo A G and Hollenkamp A F 2006 Carbon properties and their role in supercapacitors *J. Power Sources* **157** 11–27

[9] Lu Z, Foroughi J, Wang C, Long H and Wallace G G 2018 Superelastic Hybrid CNT/Graphene Fibers for Wearable Energy Storage *Adv. Energy Mater.* **8** 1–10
[10] Zhu Y, Murali S, Stoller M D, Ganesh K J, Cai W, Ferreira P J, Pirkle A, Wallace R M, Cychosz K A, Thommes M, Su D, Stach E A and Ruoff R S 2011 Carbon-Based Supercapacitors Produced by Activation of Graphene *Science (80-.).* **332** 1537–42
[11] Palisoc S, Dungo J M and Natividad M 2020 Low-cost supercapacitor based on multi-walled carbon nanotubes and activated carbon derived from Moringa Oleifera fruit shells *Heliyon* **6** e03202
[12] Zhang B, Piao G, Zhang J, Bu C, Xie H, Wu B and Kobayashi N 2018 Synthesis of carbon nanotubes from conventional biomass-based gasification gas *Fuel Process. Technol.* **180** 105–13
[13] He X, Li R, Han J, Yu M and Wu M 2013 Facile preparation of mesoporous carbons for supercapacitors by one-step microwave-assisted ZnCl2 activation *Mater. Lett.* **94** 158–60
[14] Barranco V, Lillo-Rodenas M A, Linares-Solano A, Oya A, Pico F, Ibañfez J, Agullo-Rueda F, Amarilla J M and Rojo J M 2010 Amorphous carbon nanofibers and their activated carbon nanofibers as supercapacitor electrodes *J. Phys. Chem. C* **114** 10302–7
[15] Rajagukguk J, Simamora P, Saragih CS, Abdullah H, Gultom NS, Imaduddin A. Superparamagnetic Behaviour and Surface Analysis of Fe_3O_4/PPY/CNT Nanocomposites. *Journal of Nanomaterials*. 2020 Oct 22;**2020**.
[16] Taer E, Apriwandi A, Ningsih Y S, Taslim R and Agustino 2019 Preparation of activated carbon electrode from pineapple crown waste for supercapacitor application *Int. J. Electrochem. Sci.* **14** 2462–75
[17] Yang H, Ye S, Zhou J and Liang T 2019 Biomass-derived porous carbon materials for supercapacitor *Front. Chem.* **7** 1–17
[18] Mohammed A A, Chen C and Zhu Z 2019 Low-cost, high-performance supercapacitor based on activated carbon electrode materials derived from baobab fruit shells *J. Colloid Interface Sci.* **538** 308–19
[19] Taer E, Apriwandi A, Taslim R, Malik U and Usman Z 2019 Single Step Carbonization-Activation of Durian Shells for Producing Activated Carbon Monolith Electrodes *Int. J. Electrochem. Sci.* **14** 1318–30
[20] Taer E, Dewi P, Sugianto S, Syech R, Taslim R, Salomo S, Susanti Y, Purnama A, Apriwandi A, Agustino A and Setiadi R N 2018 The synthesis of carbon electrode supercapacitor from durian shell based on variations in the activation time *AIP Conf. Proc.* **1927** 030026–1–030026–6
[21] Taer E, Sumantre M A A, Taslim R, Dahlan D and Deraman M 2014 Eggs Shell Membrane as Natural Separator for Supercapacitor Applications *Adv. Mater. Res.* **896** 66–9
[22] Sun Q, Jiang T, Zhao G and Shi J 2019 Porous carbon material based on biomass prepared by MgO template method and ZnCl2 activation method as electrode for high performance supercapacitor *Int. J. Electrochem. Sci.* **14** 1–14
[23] Men B, Guo P, Sun Y, Tang Y, Chen Y, Pan J and Wan P 2019 High-performance nitrogen-doped hierarchical porous carbon derived from cauliflower for advanced supercapacitors *J. Mater. Sci.* **54** 2446–57
[24] Fan Y, Cai Y, Li X, Jiao L, Xia J and Deng X 2017 Effects of the cellulose, xylan and lignin constituents on biomass pyrolysis characteristics and bio-oil composition using the Simplex Lattice Mixture Design method *Energy Convers. Manag.* **138** 106–18
[25] Gonzalez J ., Roma S, Encinar J M and Martı G 2009 Pyrolysis of various biomass residues and char utilization for the production of activated carbons *J. Anal. Appl. Pyrolysis* **85** 134–41
[26] González P G and Pliego-Cuervo Y B 2013 Physicochemical and microtextural characterization of activated carbons produced from water steam activation of three bamboo species *J. Anal. Appl. Pyrolysis* **99** 32–9
[27] Su X, Li S, Jiang S, Peng Z, Guan X and Zheng X 2018 Superior capacitive behavior of porous

activated carbon tubes derived from biomass waste-cotonier strobili fibers *Adv. Powder Technol.* **29** 2097–107

[28] Ramesh T, Rajalakshmi N, Dhathathreyan K S and Reddy L R G 2018 Hierarchical porous carbon microfibers derived from Tamarind seed coat for high-energy supercapacitor application *ACS Omega* 12832–40

[29] Taer E, Apriwandi A, Yusriwandi Y, Mustika W S, Zulkifli Z, Taslim R, Sugianto S, Kurniasih B, Agustino A and Dewi P 2018 Comparative study of CO2 and H2O activation in the synthesis of carbon electrode for supercapacitors *AIP Conf. Proc.* **1927** 030036–1–030036–6

[30] Farma R, Deraman M, Awitdrus A, Talib I A, Taer E, Basri N H, Manjunatha J G, Ishak M M, Dollah B N M and Hashmi S A 2013 Preparation of highly porous binderless activated carbon electrodes from fibres of oil palm empty fruit bunches for application in supercapacitors *Bioresour. Technol.* **132** 254–61

[31] Taer E, Natalia K, Apriwandi A, Taslim R, Agustino A and Farma R 2020 The synthesis of activated carbon nano fiber electrode made from acacia leaves (Acacia mangium wild) as supercapacitors *Adv. Nat. Sci. Nanosci. Nanotechnol.* **11** 25007

[32] Kumar K, Saxena R K, Kothari R, Suri D K, Kaushik N K and Bohra J N 1997 Correlation between adsorption and x-ray diffraction studies on viscose rayon based activated carbon cloth *Carbon N. Y.* **35** 1842–4

[33] Deraman M, Daik R, Soltaninejad S, Nor N S M, Awitdrus, Farma R, Mamat N F, Basri N H and Othman M A R 2015 A New Empirical Equation for Estimating Specific Surface Area of Supercapacitor Carbon Electrode from X-Ray Diffraction *Adv. Mater. Res.* **1108** 1–7

[34] Faraji S and Nasir F 2015 The development supercapacitor from activated carbon by electroless plating — A review *Renew. Sustain. Energy Rev.* **42** 823–34

[35] Zhang Y, Li X, Huang J, Xing W and Yan Z 2016 Functionalization of Petroleum Coke-Derived Carbon for Synergistically Enhanced Capacitive Performance *Nanoscale Res. Lett.* **11** 1–7